





Analytical Methods Hot Paper

How to cite: Angew. Chem. Int. Ed. 2022, 61, e202203826 doi.org/10.1002/anie.202203826 International Edition: German Edition: doi.org/10.1002/ange.202203826



Amplification-Free Detection of SARS-CoV-2 and Respiratory Syncytial Virus Using CRISPR Cas13a and Graphene Field-Effect **Transistors**

Huijie Li⁺, Jie Yang⁺, Guangfu Wu⁺, Zhengyan Weng⁺, Yang Song, Yuxuan Zhang, Jeffrey A. Vanegas, Lori Avery, Zan Gao, He Sun, Yupeng Chen, Kevin D. Dieckhaus, Xue Gao,* and Yi Zhang*

Abstract: The clustered regularly interspaced short palindromic repeats (CRISPR)/CRISPR-associated (Cas) systems have recently received notable attention for their applications in nucleic acid detection. Despite many attempts, the majority of current CRISPR-based biosensors in infectious respiratory disease diagnostic applications still require target preamplifications. This study reports a new biosensor for amplification-free nucleic acid detection via harnessing the trans-cleavage mechanism of Cas13a and ultrasensitive graphene field-effect transistors (gFETs). CRISPR Cas13a-gFET achieves the detection of SARS-CoV-2 and respiratory syncytial virus (RSV) genome down to 1 attomolar without target preamplifications. Additionally, we validate the detection performance using clinical SARS-CoV-2 samples, including those with low viral loads (Ct value > 30). Overall, these findings establish our CRISPR Cas13a-gFET among the most sensitive amplification-free nucleic acid diagnostic platforms to date.

Introduction

The clustered regularly interspaced short palindromic repeats (CRISPR)/CRISPR-associated (Cas) system, first discovered from adaptive bacterial immunity,[1] has become one of the most powerful technologies at the interface of engineering and molecular biology. [2] The most widely used CRISPR-Cas9 system can target double-stranded DNA while Cas12a recognizes both single- and double-stranded DNA and Cas13a detects single-stranded RNA. The nucleic acid-targeting capability of CRISPR/Cas systems has enabled applications beyond genome editing.^[3] Most recently, the discovery of the trans-cleavage mechanism in various CRISPR/Cas orthologs, including Cas12a and Cas13a, has made it possible to develop biosensors for nucleic acid detections. [3b,c,4] Specifically, after completing their targetspecific DNA or RNA cleavage activities, the trans-cleavage

mechanism of Cas12a and Cas13a endonucleases leads to the further cleavage of any available non-targeted singlestranded DNA (ssDNA; Cas12a) or RNA (ssRNA; Cas13a) quenched fluorescent or colorimetric reporters in a sequence-independent manner,[5] thereby enabling the development of fluorescent or colorimetric biosensors. [6]

Despite leveraging the multiple turnover nature of Cas12a and Cas13a trans-cleavage mechanism, the majority of current CRISPR-based detection platforms, including DETECTR,[3a,8] SHERLOCK,[7] miSHERLOCK,[9] STOPCovid[10] and CRISPR-FDS,[11] still rely on preamplification of the target nucleic acids by either polymerase chain reaction (PCR) or isothermal amplification processes (e.g., recombinase polymerase amplification, RPA, or loopmediated isothermal amplification, LAMP) (Table S1). Compared with PCR, the isothermal amplification process with RPA or LAMP is less instrument intensive and

[*] H. Li,+ Dr. G. Wu,+ Z. Weng,+ Dr. Y. Song, Y. Zhang, Dr. Z. Gao,

H. Sun, Prof. Y. Chen, Prof. Y. Zhang

Department of Biomedical Engineering,

University of Connecticut

Storrs, CT 06269 (USA)

E-mail: yi.5.zhang@uconn.edu

H. Li,+ Dr. G. Wu,+ Z. Weng,+ Dr. Y. Song, Y. Zhang, Dr. Z. Gao,

H. Sun, Prof. Y. Zhang

Institute of Materials Science,

University of Connecticut

Storrs, CT 06269 (USA)

Dr. J. Yang, J. A. Vanegas, Prof. X. Gao

Department of Chemical and Biomolecular Engineering,

Rice University

Houston, TX 77005 (USA)

E-mail: xue.gao@rice.edu

L. Avery

Department of Pathology and Laboratory Medicine,

UConn Health

Farmington, CT 06030 (USA)

Prof. K. D. Dieckhaus

Division of Infectious Diseases,

Department of Medicine, UConn Health

Farmington, CT 06030 (USA)

Prof. X. Gao

Department of Bioengineering, Rice University

Houston, TX 77005 (USA)

Department of Chemistry, Rice University

Houston, TX 77005 (USA)

[+] These authors contributed equally to this work.





simpler. Nevertheless, the isothermal amplification process often requires a set of proteins (polymerase, recombinase, or binding proteins) and primers (2 primers for RPA and 4 to 6 primers for LAMP) and additional sample preparation steps, which dramatically complicates and lengthens the detection process (20 min–2 hours), as well as increases the contamination risk of patient samples. In addition, the target preamplification process is usually nonlinear and reaches saturation rapidly, [7,12] limiting the ability to quantitatively measure viral copy numbers for predicting and/or monitoring disease progression. [13] Finally, the isothermal amplification process could generate nonspecific-amplification products and sacrifice the detection specificity, though CRISPR is known to have high specificity.

To overcome these limitations, recent studies have demonstrated a set of amplification-free CRISPR-based biosensors, including E-CRISPR,[14] CRISPR/Cas13a-powered electrochemical microfluidic biosensor^[4d] and CRISPRmobile phone microscope, [15] via coupling CRISPR with electrical^[16] and electrochemical^[4d,14] transducers, or by utilizing multiple CRISPR RNAs (crRNAs)^[15] (Table S1). The reported limit of detection (LOD) for these amplification-free CRISPR-based biosensors is in the femtomolar to picomolar range (0.166 fM to $50 \, pM$), [4d,14,15] which is 10^2 to 107-fold less sensitive than the current quantitative reverse transcription-PCR (RT-qPCR) method. This LOD allows for the detection of highly concentrated nucleic acid samples, including microRNAs and HPV-16[4d,14] or SARS-CoV-2 samples with a relatively low Ct value (14.37-22.13).^[15] Most clinical applications, however, require the detection of nucleic acid concentrations down to the attomolar level, such as antiviral therapy for Hepatitis C and HIV viruses^[17] and infectious disease diagnostics.^[18] For example, a recent study shows that about50% of 4744 SARS-CoV-2 patients exhibit a viral load below 100 attomolar (60.2 copies/µL). [18b] Similarly, while a previous study demonstrated an amplification-free CRISPR Cas9gFET chip for the detection of human genomic DNA from cell lines and Duchenne muscular dystrophy (DMD) patients. [16] the limited sensitivity (LOD: 1.7 fM) does not meet the high standard of attomolar detection of nucleic acid samples for infectious disease diagnostics, like the diagnostics of SARS-CoV-2.[18b] In addition, the CRISPR Cas9-gFET chip is designed to analyze DNA samples and requires a lengthy and complicated reverse transcription step to detect the viral RNA of SARS-CoV-2.

In this study, we developed a new CRISPR Cas13a-gFET biosensor that harnesses the trans-cleavage mechanism of CRISPR Cas13a and the graphene field-effect transistor (gFET) for amplification-free detection of nucleic acids with a LOD down to the attomolar range (1 aM or 0.6 copy/μL) within a 30 min assay incubation time, which is comparable to the gold-standard RT-qPCR but with a much shorter detection time. Experience with the ultrasensitive detection of two different RNA samples (SARS-CoV-2 and RSV) demonstrates the versatility and broad applications of CRISPR Cas13a-gFET in detecting various RNA samples. We also validated the performance using clinical SARS-

CoV-2 nasal swab samples and showed a sensitivity comparable to that of RT-qPCR.

Results and Discussion

Design and Fabrication of CRISPR Cas13a-gFET for Nucleic Acid Detection

We designed an ultrasensitive and amplification-free nucleic acid detection platform via the synergy of the trans-cleavage mechanism of CRISPR Cas13a and ultrasensitive gFET (Figure 1A). A FET is a three-terminal electronic device, in which the gate electrode applies an external electric field to regulate the source-drain current passing through the semiconductor channel^[19] (Figure S1). Graphene is considered a zero-gap material, and it has an exceptionally high carrier mobility (>1000 cm²V⁻¹s⁻¹). The high carrier mobility, along with the atomic thickness of graphene,^[20] allows the gFET to be highly sensitive to the interaction with biological analytes.^[21] We chose Cas13a endonuclease from *Leptotrichia wadei* (LwaCas13a) to develop the CRISPR Cas13a-gFET platform, as it has been previously reported for RNA detection due to high targeting efficiency.^[7]

To allow for multiple parallel detections with single sample input and eliminate the potential false-positive and false-negative results due to sensor-to-sensor variations, we fabricated a device consisting of an array of six CRISPR Cas13a-gFETs on a silicon wafer (Figure 1A and B). We defined the contact pad patterns of source and drain electrodes by photolithography and metal deposition (Figure S2). Graphene was then transferred onto the device using poly (methyl methacrylate) (PMMA) as a support layer to minimize the formation of cracks and wrinkles during the transfer process. Finally, we encapsulated the gFET array with SU-8 2000.5 photoresist (Kayaku Advanced Materials, Westborough, MA, USA) to prevent source-drain current leakage (Figure S2). A non-polarizable Ag/AgCl reference electrode was used as the gate electrode for stable signal responses. [20] An SEM image of a representative gFET is shown in Figure 1C.

Working Principle of CRISPR Cas13a-gFET for Nucleic Acid Detection

Different from the previously reported CRISPR Cas9-gFET chip that relies on the binding of the target to dCas9-crRNA complex functionalized on the gFET for sensor signal transduction (binding-based CRISPR diagnostics), [22] CRISPR Cas13a-gFET relies on the Cas13a-mediated RNA trans-cleavage on gFET for sensor signal transduction (cleavage-based CRISPR diagnostics). The multi-turnover trans-cleavage results in the high-speed generation of sensor signals, [7,23] compared to the single turnover dCas9-induced sensor signal transduction, [16] thereby enabling the ultrasensitive detection of nucleic acid samples. More specifically, the CRISPR Cas13a-gFET platform for nucleic acid detection is based on the positive shift of the charge neutrality

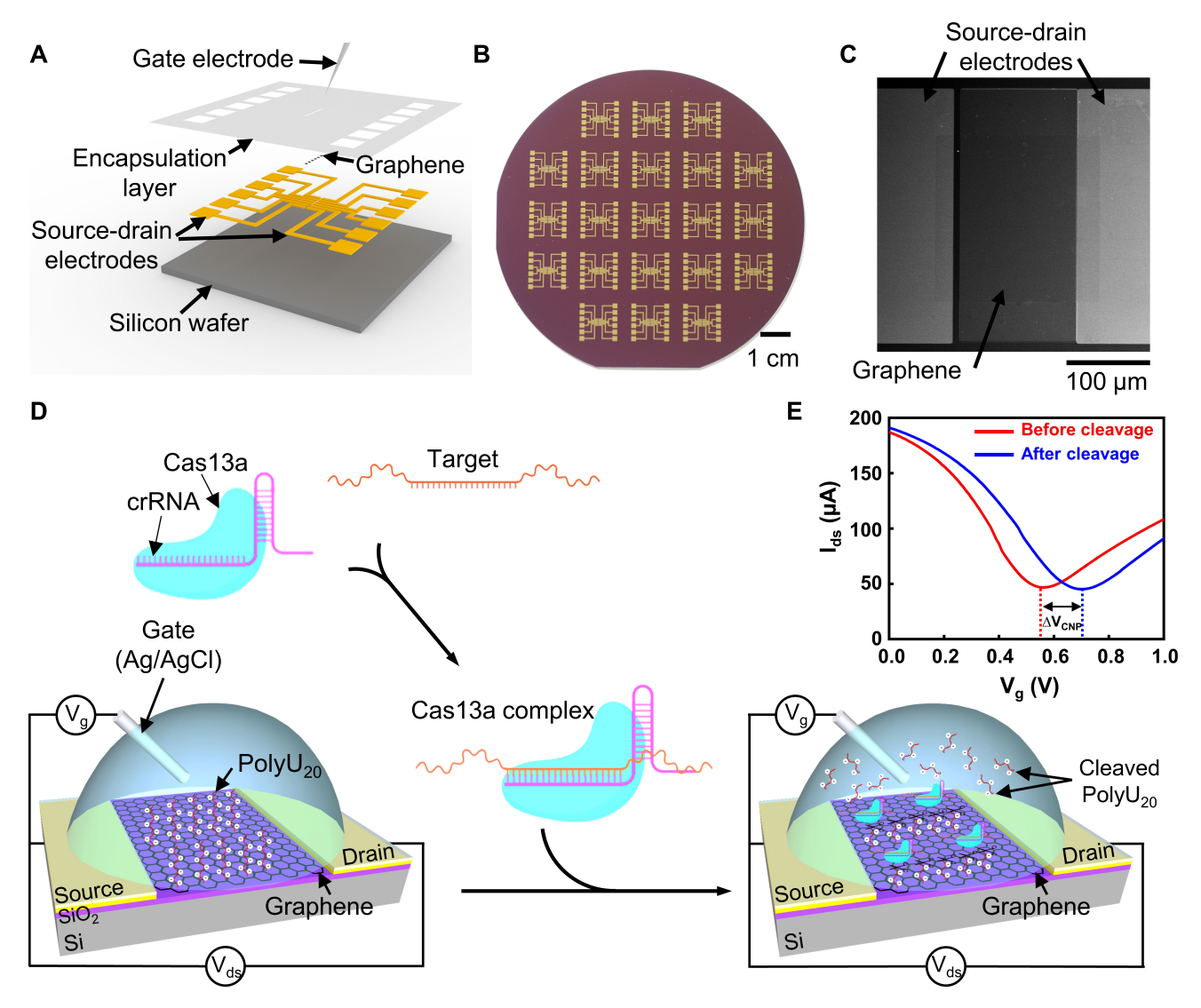


Figure 1. Schematic illustration, optical images, and working principle of CRISPR Cas13a-gFET for amplification-free and ultrasensitive detection of RNA samples. A) Schematic illustration of an array of six gFETs. A non-polarizable Ag/AgCl reference electrode is used as the gate electrode for stable signal responses. B) Optical image of 21 gFET arrays on a 4-inch silicon wafer. C) SEM image of a gFET, including source-drain electrodes and a graphene channel layer. D) Working principle of CRISPR Cas13a-gFET for amplification-free detection of RNA samples. E) Representative transfer characteristics readout of CRISPR Cas13-gFET before and after adding the target sequences (SARS-CoV-2 N gene, 1 fM). For the acquisition of transfer characteristics, we monitored the source-drain current (I_{ds}) while keeping a constant source-drain voltage (V_{g}) from -1 to 1 V with steps of 10 mV.

point voltages (V_{CNP}), also called the Dirac point, of the gFET, in which the gFET is initially functionalized with a negatively charged RNA reporter ($PolyU_{20}$) via a molecular linker, 1-pyrenebutanoic acid succinimidyl ester (PBASE). Upon the introduction of the targeted nucleic acid sequence, the trans-cleavage activity of Cas13a endonucleases is triggered through complementary recognition with the crRNA; The negatively charged $PolyU_{20}$ reporters are then cleaved off from the gFET by these endonucleases, resulting in reduced electron transfer from the RNA phosphate backbones to the graphene channel (Figure 1D). Consequently, a decrease in the number of electron carriers in the graphene channel is observed, leading to p-doping of the gFET channel and a right shift of V_{CNP} . The magnitude of

the shift, as a result of target-triggered trans-cleavage of surface reporters, can be correlated with target concentrations, therefore enabling quantitative determination of nucleic acid target sequences by CRISPR Cas13a-gFET.

Here, we chose the shift of $V_{\rm CNP}$, the most commonly used electrical metric in FET biosensing, instead of the real-time monitoring of source-drain current ($I_{\rm ds}$) at a given gate voltage mainly because the change of $I_{\rm ds}$ could be contributed from either the change of charge carrier density or the transconductance and thus difficult to interpret when testing the complex clinical samples. ^[24] The changes in $V_{\rm CNP}$ were characterized by percentage shifting of charge neutrality point before ($V_{\rm CNP,0}$) and after ($V_{\rm CNP}$) the addition of target, calculated as:





$$\Delta V_{\rm CNP}~(\%) = (V_{\rm CNP} - V_{\rm CNP,0}) / V_{\rm CNP,0} \times 100 \eqno(1)$$

In this study, considering the ongoing pandemic of coronavirus disease 2019 (COVID-19) and the need for a highly sensitive and amplification-free nucleic detection platform for COVID-19 diagnosis, we selected SARS-CoV-2 N gene as a model nucleic acid target. A representative measurement of transfer characteristics before and after gFET incubation in a CRISPR assay solution with the target sequence (SARS-CoV-2 N gene, 1 fM) for 30 minutes is shown in Figure 1E. Consistent with our hypothesis, a positive $V_{\rm CNP}$ shift was observed after the trans-cleavage of PolyU₂₀ reporters in the presence of SARS-CoV-2 N gene synthetic targets, indicating the p-doping effect due to cleaved PolyU₂₀ reporters.

Functionalization of PolyU20 Reporters on gFET

We used a molecular linker, PBASE, to functionalize $PolyU_{20}$ reporters on the surface of the graphene channel. PBASE was chosen because the planar pyrene ring in PBASE can bind to graphene via noncovalent π - π stacking, $I^{[20]}$ which can prevent the introduction of defects to graphene and maintain the high carrier mobility of pristine graphene. More specifically, the graphene channel of gFET was first functionalized with PBASE, and then incubated with 5'-amino-modified $I^{[20]}$ reporters (5'-NH₂-UUU UUU UUU UUU UUU UUU UU-3'), in which the amino group reacts with amino-reactive succinimidyl ester to immobilize these reporters on the graphene surface. We used single-stranded $I^{[20]}$ as the reporters because $I^{[20]}$ LwaCas13a has demonstrated the dinucleotide cleavage preference of $I^{[20]}$

To verify the functionalization of PolyU₂₀ reporters on the graphene surface, we first measured the Raman spectra of the graphene channel before and after the PBASE modification (Figure S3). A new peak at 1624.2 cm⁻¹ after the PBASE functionalization was observed due to pyrene group resonance. In addition, the intensity ratio of graphene characteristic 2D and G peaks (I_{2D}/I_{G}) decreased from 2.18 to 1.83 after PBASE functionalization, indicating the presence of the doping effect on graphene. [20] The PolyU₂₀ reporter surface functionalization was further investigated by monitoring the source-drain current (I_{ds}) while keeping a constant source-drain voltage ($V_{ds} = 100 \text{ mV}$) and sweeping the gate voltage (V_{σ}) from -1 to 1 V with steps of 10 mV. A p-doping effect (right shift of transfer curve) was observed because of the electron-withdrawing ester group in the PBASE (Figure S4). After the functionalization of PolyU₂₀ reporters on gFET through PBASE linkers, we observed a slight left shift of the transfer curve mainly due to the electron transfer from the RNA phosphate backbones to the graphene channel (Figure S5).

The performance of our CRISPR Cas13a-gFET may be compromised due to the complicated sensing environment where a variety of biomolecules, including viral RNAs and proteins, are present. To address this issue, we blocked the

unfunctionalized graphene surface with 1 mM amino-PEG5-alcohol and 1 M ethanolamine hydrochloride to prevent the non-specific binding of charged molecules.^[16]

Development of CRISPR Cas13a Assay for SARS-CoV-2 and RSV Detection

Both SARS-CoV-2 and RSV are RNA viruses that have high mutation rates. Thus, it is essential to target the highly conserved regions on the RNA genome for accurate detection. The N gene of SARS-CoV-2 encoding the nucleocapsid protein is highly conserved and exhibits high transcriptional abundances, serving as a target for gold standard RT-qPCR diagnostics. The RSV M gene encoding the matrix protein is the most conserved region of the RSV RNA genome. [25] Therefore, we chose the US CDC RT-qPCR amplicon sequences from these two genes, i.e., the SARS-CoV-2 N1 and N2 amplicons[26] and the RSV M amplicon[25] (Figure 2A–C). To target these three amplicons, a total of six guide sequences were designed (Figure 2A–C) and gel purified (Figure S6) for fluorescence plate reader assays.

To select the best crRNA sequence for SARS-CoV-2 detection, we measured the time course of fluorescence (Figure 2D–I). We also compared the signal-to-background (S/B) ratio (Figure 2J), the 30 min background-subtracted fluorescence signal (Figure 2K), and the initial velocity of reporter cleavage (Figure 2L). The N1 crRNA showed the highest S/B ratio and RSV showed the highest cleavage rate. These two crRNAs, therefore, were chosen for the following studies.

Optimization of CRISPR Cas13a-gFET Conditions for SARS-CoV-2 Detection

The CRISPR reaction conditions, such as CRISPR assay incubation time, temperature, Mg2+ concentration, Cas13a endonuclease concentration, and reporter length, may affect the performance of CRISPR Cas13a-gFET for nucleic acid detection. Therefore, to achieve optimal sensitivity, we varied these operation conditions for our CRISPR Cas13agFET platform. As a starting point, we referred SHER-LOCK components^[7,12] to assemble the CRISPR assay (Table S2) and set the reaction conditions as: 1) 30 min incubation time, 2) room temperature, 3) 9 mM Mg²⁺, 4) 45 nM LwaCas13a, and 5) PolyU₂₀ reporters. All assays with varied conditions were tested against 1 fM synthetic SARS-CoV-2 N gene target spiked into nuclease-free water. We first investigated assay incubation time as increased incubation time will allow for more trans-cleavage events, generating a larger signal response. The change in V_{CNP} shift increased with increasing incubation time up to 2 hours (Figure 3A, Figures S7-S11). From the perspective of future point-of-care applications, a rapid detection with high sensitivity is desired. To that end, we explored the possibility of using a higher reaction temperature (37 °C) to shorten the assay incubation time, thereby enabling rapid detection. As





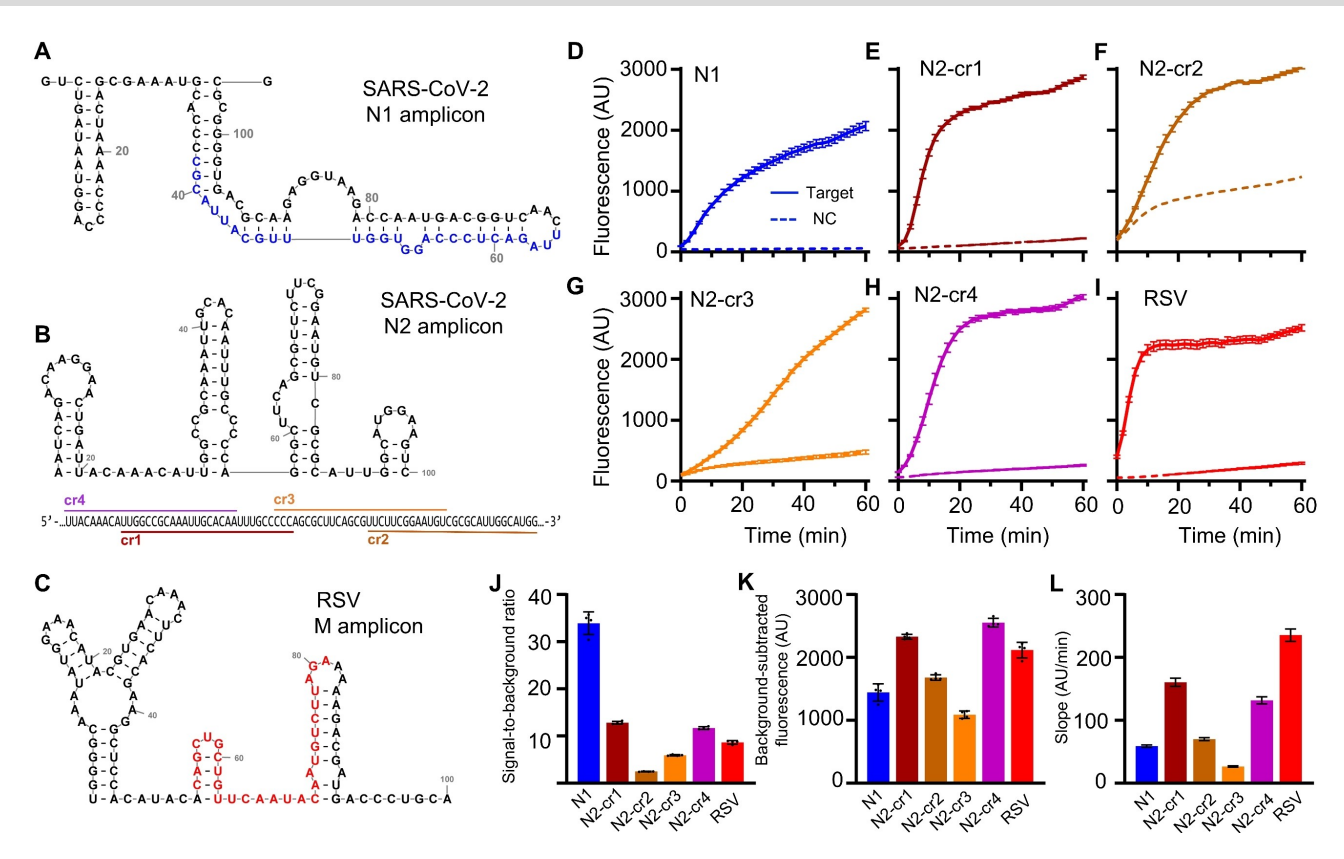


Figure 2. Development of CRISPR Cas13a assay for SARS-CoV-2 and RSV detection. US CDC SARS-CoV-2 N gene RT-qPCR amplicon A) (N1) and B) (N2) serves as synthetic RNA target for CRISPR-based detection. C) US CDC RSV M gene RT-qPCR amplicon serves as a synthetic RNA target for CRISPR-based detection. For (A), (B) and (C), the structures of RNA targets were predicted using RNAfold web server and drawn using RNA2Drawer. The crN1 targeting sequence was labeled blue and the crRSV targeting sequence was labeled red. D)–I) Raw fluorescence (arbitrary unit, AU) over 60 min in reactions with crN1 (D), crN2-1 (E), -2 (F), -3 (G), -4 (H) and crRSV (I). The concentration of three synthetic RNA targets is 100 pM. J) Signal-to-background ratio at 60 min. K) 30 min background-subtracted fluorescence (AU) from panel (D)–(I). L) Initial reaction velocities were calculated from panel (D)–(I) fluorescence signal within linear range by simple linear regression. For (D)–(I), Data are represented as mean \pm s.e.m. from four technical replicates. For (L), Data from (D)–(I) were fit into simple linear regression and represented as mean \pm s.e.m.

shown in Figure 3B, compared with CRISPR Cas13a-gFET detection at room temperature, incubation at 37 °C generates enhanced $V_{\rm CNP}$ shifts. Importantly, a significant $V_{\rm CNP}$ shift was observed as soon as 5 minutes between negative control (NC) and 1 fM synthetic SARS-CoV-2 target (**p<0.01, Figure 3C). In contrast, we observed a significant sensor signal difference after 15 min at room temperature (*p<0.05, Figure S12). These initial studies suggest the possibility of shortening the detection time by operating the CRISPR Cas13a-gFET at 37 °C. Considering the need for a heating setup to operate at 37 °C and 30 min incubation time at room temperature provided sufficient $V_{\rm CNP}$ shift for the CRISPR Cas13a-gFET platform (***p<0.001, Figure S12), a 30 min incubation duration at room temperature was used for the further experimental setup.

We then evaluated the effect of Mg²⁺ concentration on the detection performance of CRISPR/Cas13a-gFET because Mg²⁺ ions are an essential cofactor for the activation of Cas13a trans-cleavage activity.^[5] The Cas13a assay exhibited a significantly greater trans-cleavage activity at higher Mg²⁺ concentrations, with the signal response peaking at 9 mM (Figure 3D, Figures S13–S17). It should be

noted that a background shift in V_{CNP} was observed in the absence of Mg^{2+} , possibly due to the physical adsorption of CRISPR assay residues on the graphene surface.

CRISPR Cas13a mediates the target-triggered transcleavage of bystander reporters, so the concentration of Cas13a endonuclease directly governs the biosensing efficiency through two key elements of biosensors, 1) biorecoggnition via capture of target sequences by Cas13a-crRNA complexes and 2) signal transduction via reporter cleavage into electrical responses. We varied the concentration of Cas13a endonuclease from 5 nM to 85 nM while keeping the molar ratio of Cas13a to crRNA constantly at 2:1. The CRISPR Cas13a-gFET signal responses were maximized at 45 nM LwaCas13a, with lower V_{CNP} shifts below and above this concentration (Figure 3E, Figures S18-S22). At low concentrations of LwaCas13a, trans-cleavage of reporters would be limited by the number of available Cas13a endonucleases for the reaction.^[14] However, at high concentrations of LwaCas13a, the assay performance would be hindered by the large size of LwaCas13a-crRNA complexes, which reduces the rate of target sequence binding and the diffusion rate of Cas13a complexes toward reporters on the





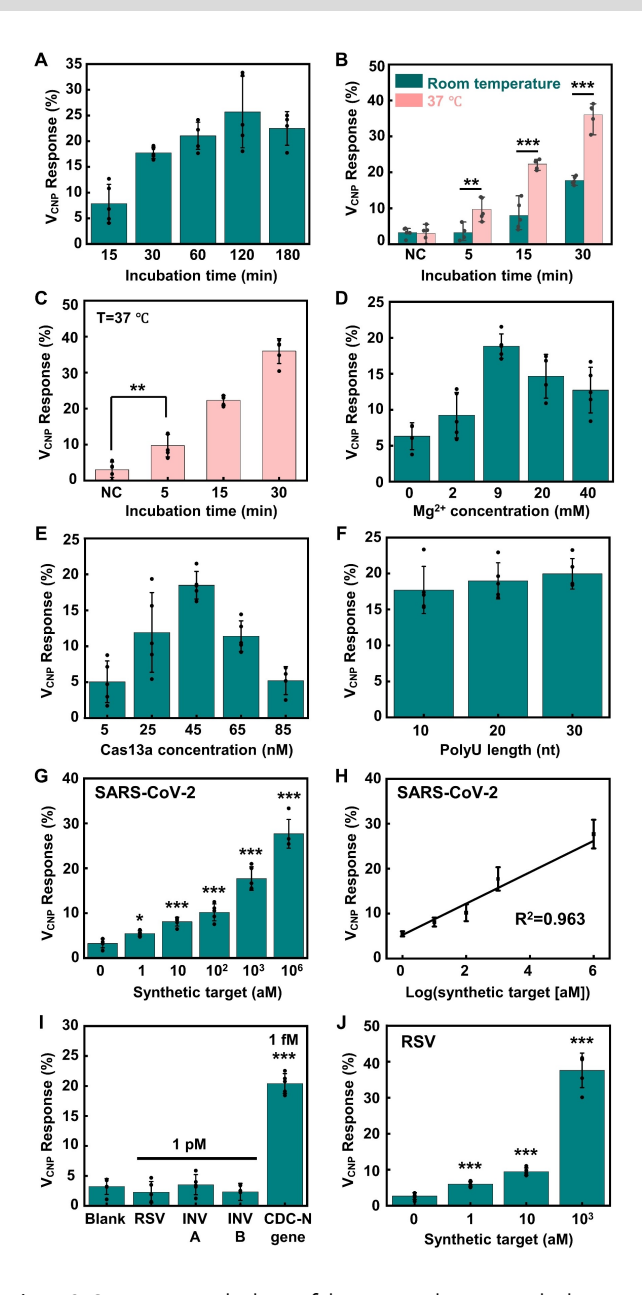


Figure 3. Optimization, the limit of detection, selectivity, and adaptability of CRISPR Cas13a-gFET. Effect of (A) assay incubation time, B) temperature, D) magnesium ion (Mg²⁺⁾ concentration, E) Cas13a concentration, and F) reporter length on the performance of CRISPR Cas13a-gFET ($n \ge 4$). 1 fM synthetic SARS-CoV-2 N gene target spiked into nuclease-free water was used. C) Statistical significance analysis between negative control (NC) and 1 fM synthetic SARS-CoV-2 targets with different incubation time at 37 °C (n = 5, **p < 0.01). G) Change in V_{CNP} at different concentrations of SARS-CoV-2 N gene synthetic targets spiked into water (n=5, *p<0.05, ***p<0.001). H) Calibration curve for CRISPR Cas13a-gFET to detect SARS-CoV-2 N gene synthetic target. I) Selectivity of CRISPR Cas13a-gFET against viruses that may cause similar symptoms with that of SARS-CoV-2 (n=5, ***p < 0.001). The CRISPR Cas13a-gFET platform can distinguish between the SARS-CoV-2 N gene target and three orders of magnitude higher concentration of non-target sequences. J) Change in V_{CNP} at different RSV concentrations (n=5, ***p < 0.001). The CRISPR Cas13a-gFET can detect down to 1 aM synthetic RSV target fragments.

graphene surface, eventually decreasing target-induced trans-cleavage events.

Finally, we examined the effect of PolyU reporter length on the trans-cleavage activity of Cas13a endonuclease for gFET detection of the SARS-CoV-2 N gene target. Short reporters may cause steric hindrance, preventing access of Cas13a endonuclease to the reporters immobilized on the surface of graphene. On the other hand, long reporters may limit gFET signal transduction and sensitivity due to the Debye screening effect. [20] However, $V_{\rm CNP}$ shift responses showed negligible variations across 10 nt, 20 nt, and 30 nt PolyU reporters (Figure 3F, Figures S23-S25). Hence, reporter length is not a critical factor affecting CRISPR Cas13a-gFET transfer characteristics. This observation agrees with the previously developed CRISPR Cas12aelectrochemical sensor that uses Cas12a endonucleases. [14] Considering that PolyU₁₀ shows a larger signal variation (standard deviation, 3.28 %) and PolyU₃₀ reporters are more expensive than $PolyU_{20}$, $PolyU_{20}$ reporter was selected for further device preparation.

Detection of Synthetic SARS-CoV-2 Targets Using CRISPR Cas13a-gFET

Given the optimized assay conditions (30 min incubation time, room temperature, 9 mM ${\rm Mg^{2+}}$, 45 nM LwaCas13a, and PolyU₂₀ reporter), we performed the SARS-CoV-2 detection using synthetic SARS-CoV-2 N gene targets spiked into nuclease-free water ranging from 1 aM to 1 pM. The CRISPR Cas13a-gFET was able to detect the target sequence down to 1 aM level (Figure 3G, Figures S26–S31). This high sensitivity is attributed to the integration of ultrasensitive gFET with the multi-turnover trans-cleavage activity of Cas13a endonuclease. The calibration curve for the CRISPR Cas13a-gFET $V_{\rm CNP}$ shift suggests that the signal response can be directly correlated with viral copy numbers (Figure 3H), which can be used for quantitatively monitoring viral loads. [13]

SARS-CoV-2 is expected to remain and continue in the future fall/winter seasons, when it will coincide with the seasonal outbreak of other infectious respiratory diseases, including those caused by influenza virus (INV) and RSV, which have similar signs and symptoms in the early stages. Considering the overlap in the seasonal peaks, symptoms, and underlying risk factors of these illnesses, having a sensor to quickly differentiate SARS-CoV-2 from INV and RSV will be clinically useful. To this end, we assessed the selectivity of CRISPR Cas13a-gFET by testing against RSV, INV A, and INV B synthetic targets. $V_{\rm CNP}$ shifts from 1 pM non-target viral sequences were similar to those from negative controls and significantly lower than signals from that of three orders of magnitude lower concentration of SARS-CoV-2 N gene sequence (1 fM, Figure 3I, Figures S32-S36), so we concluded that the CRISPR Cas13agFET platform was capable of distinguishing between SARS-CoV-2 N gene target and non-target sequences. These results demonstrated the high selectivity of CRISPR Cas13a-gFET platform for nucleic acid detection.





Nucleic Acid Detection Beyond SARS-CoV-2 Using CRISPR Cas13a-gFET

The configurability of CRISPR Cas13a systems to detect different viral RNA targets, simply by changing crRNA guide sequences, makes our CRISPR Cas13a-gFET platform highly adaptable. To show the ability of CRISPR Cas13a-gFET to detect RNA targets beyond SARS-CoV-2, we expanded this amplification-free method to detect another respiratory virus, RSV, by re-designing RSV-targeting crRNA (Table S3). Similar to SARS-CoV-2 detection, CRISPR Cas13a-gFET was capable of detecting 1 aM synthetic RSV target fragments (Figure 3J, Figures S37–S40), demonstrating the universal ultrasensitivity of our platform in RNA detection.

Validation of Detection Performance Using Heat-Inactivated and Clinical SARS-CoV-2 Samples

To evaluate the performance of CRISPR Cas13a-gFET for potential clinical applications, we first prepared viral lysates using heat-inactivated SARS-CoV-2 (ATCC, VR-1986HK™, Manassas, VA, USA) spiked into 10 mM Tris buffer (pH 8.0). In our study, the SARS-CoV-2 genomic RNA was extracted by heating at 95 °C for 5 min, along with QuickExtract™ DNA extraction solution (Lucigen, Middleton, WI, USA) (Figure 4A). The Quick Extract solution is used as a lysis buffer due to its efficient lysis of viruses while not interfering with the trans-cleavage efficiency of the CRISPR assay. [10] The CRISPR Cas13a-gFET shows a limit of detection of 1 aM using heat-inactivated virus samples (Figure 4B, Figures S41–S44), which is consistent with the performance of the CRISPR Cas13a-gFET system for detecting synthetic viral RNA targets.

We finally validated our CRISPR Cas13a-gFET platform using clinical SARS-CoV-2 nasal swab samples stored in a viral transport medium (Figure 4C, Figures S45-S58). The threshold between positive and negative clinical samples was defined as two standard deviations ($\sigma_0 = 1.27 \%$) above the mean ($\mu_0 = 3.09 \%$) of V_{CNP} shifts obtained from negative clinical samples^[27] (Figure 4D). With this cut-off value (μ_0 + $2\sigma_0$, 5.63%), Cas13a-gFET clearly distinguishes between all nine positive and five negative clinical samples (Figure 4D), indicating that our device can be of clinical importance for the detection of SARS-CoV-2. In the meanwhile, we measured the Ct values of these clinical samples by using gold-standard RT-qPCR (CDC N gene primer), resulting in Ct values in the range from 22.89 to 35.62 for positive samples (Figure 4E) and Ct values >40 for negative nasal swab samples (Figure 4F). Notably, our Cas13a-gFET is able to detect clinical positive SARS-CoV-2 samples with a low viral load (RT-qPCR Ct value > 35; P9 sample, with a viral copy number of 1.38 copy/µL or 2.28 aM in Cas13a-gFET reaction), which is comparable to the detection limit of RTqPCR. Figure 4G shows the RT-qPCR Ct values of clinical positive SARS-CoV-2 samples plotted against Cas13a-gFET readout, suggesting the concentration-dependent semiquantitative results. Overall, these studies using SARS-CoV-2 virus samples further highlight the capability of the CRISPR Cas13a-gFET system for ultrasensitive viral RNA detection in a complex sample matrix without the need for target preamplification (Figure 4H).

Conclusion

Current CRISPR-based biosensors often require nucleic acid preamplification in many clinical applications. Different from these existing CRISPR-based biosensors, the CRISPR Cas13a-gFET platform enables the detection of both synthetic SARS-CoV-2 target and heat-inactivated virus samples with attomolar sensitivity within 30 min assay incubation time without target preamplifications. The CRISPR Cas13a-gFET platform can distinguish SARS-CoV-2 from other respiratory viruses that may cause similar symptoms, including INV and RSV. Furthermore, we validated our CRISPR Cas13a-gFET using clinical SARS-CoV-2 nasal swab samples, including those with low viral loads (RT-qPCR Ct value > 30), demonstrating a diagnostic performance comparable with that of RT-qPCR.

It should be noted that the CRISPR Cas13a-gFET biosensor is distinct from the amplification-free CRISPR Cas9-gFET chip^[16] in several ways: 1) The CRISPR Cas9-gFET chip relies on binding-based CRISPR diagnostics.^[22] In contrast, the CRISPR Cas13a-gFET system relies on the trans-cleavage mechanism of Cas13a-induced signal transduction in which PolyUs are used as sensor reporters. 2) The detection sensitivity of CRISPR Cas13a-gFET (LOD: 1 aM) is three orders of magnitude higher than that of the CRISPR Cas9-gFET chip (LOD: 1.7 fM) (Table S1 and Figure 4H), which is clinically important for infectious disease diagnostics and antiviral therapy. 3) The CRISPR Cas9-gFET chip is designed to analyze DNA samples and requires a lengthy and complicated reverse transcription step to detect viral RNA samples, such as SARS-CoV-2 samples.

The CRISPR Cas13a-gFET reported here is among the most sensitive amplification-free CRISPR Cas13a-based nucleic acid detection technologies to date (LOD: 1 aM or 0.6 copy/µL in heat-inactivated virus samples and 2.28 aM in clinical samples, within 30 min assay incubation time). This sensitivity is comparable with the gold-standard RT-qPCR (about 4 hours) but with a much shorter detection time; it is two orders of magnitude more sensitive than the CRISPR Cas13a-mobile phone microscope (0.166 fM),[15] which uses multiple crRNAs; three orders of magnitude more sensitive than the CRISPR Cas9-gFET chip (1.7 fM), [16] four orders of magnitude more sensitive than Cas13a-Nanopore, [28] and seven orders of magnitude more sensitive than E-CRISPR and CRISPR/Cas13a-powered electrochemical microfluidic biosensor (10 pM to 50 pM). [4d,14] We believe our CRISPR Cas13a-gFET platform can be adapted to detect a variety of nucleic acid targets for medical diagnostics, environmental monitoring, and food safety. It should be noted that, compared with gFET, the preparation of solid-state nanopore and screen-printed electrodes involves less timeconsuming micro-and nanofabrications. Areas for future development include 1) developing a fully functional point-





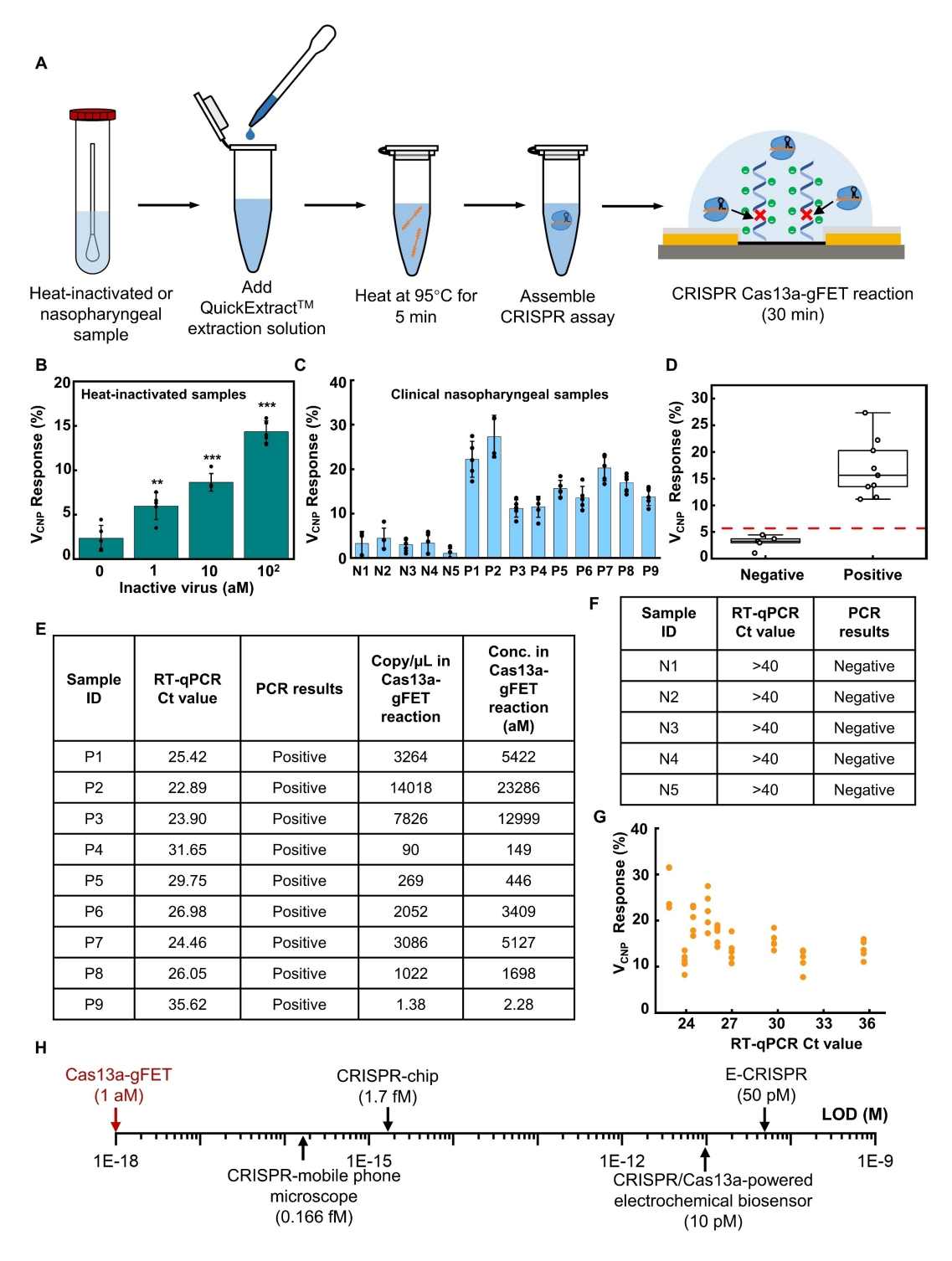


Figure 4. Validation of detection performance using heat-inactivated and clinical SARS-CoV-2 samples. A) Procedures for RNA extraction from heat-inactivated or clinical samples and subsequent RNA detection. B) Change in V_{CNP} at different concentrations of heat-inactivated SARS-CoV-2 spiked into 10 mM Tris buffer (pH 8.0). (n=5, **p<0.01, ****p<0.001). A significant difference (p<0.01) is observed between blank trial (no target) and 1 aM inactivated virus. C) Change in V_{CNP} of clinical negative and positive SARS-CoV-2 samples (N: negative sample, P: positive sample, $n\geq4$). D) The threshold V_{CNP} shift between positive and negative clinical samples was defined as two standard deviations above the mean of V_{CNP} shift obtained from negative clinical samples. The dashed red line represents the cut-off value (5.63%). The CRISPR Cas13a-gFET successfully discriminates all nine positive clinical SARS-CoV-2 nasopharyngeal swabs samples from the negative clinical samples. The mean V_{CNP} response of each clinical sample was used for the analysis. E) The Ct value (CDC N primers in RT-qPCR) and the target concentration in the Cas13a-gFET reactions of positive clinical SARS-CoV-2 samples. F) The Ct value (CDC N gene primers in RT-qPCR) of negative clinical samples. G) RT-qPCR Ct values of clinical positive SARS-CoV-2 samples plotted against Cas13a-gFET readout. H) Comparison of the limit of detection (LOD) for various CRISPR-based biosensors without target preamplifications.

OCh Res

Research Articles



of-care device, including an on-board source measurement unit, for simultaneous viral particle lysing, automatic lysed viral RNA sample manipulation, and ultrasensitive detection of SARS-CoV-2 and RSV, with only one user action (using a dropper to add samples into the device) and 2) accelerating the detection time with pulsed electrical field, [29] tandem Cas13a and Csm6 nucleases, [27] and multiple crRNAs. [15]

Acknowledgements

This work was funded by the University of Connecticut start-up fund (to Y.Z.), NSF CBET-2103025 (to Y.Z.), Rice University Startup fund (to X.G.), and NSF CBET-2031242 (to X.G.).

Conflict of Interest

The authors declare no conflict of interest.

Data Availability Statement

The data that support the findings of this study are available from the corresponding author upon reasonable request.

Keywords: Amplification-Free Detection · Biosensors · CRISPR Cas13a · Graphene Field-Effect Transistors · SARS-CoV-2

- a) Y. Ishino, M. Krupovic, P. Forterre, J. Bacteriol. 2018, 200, e00580;
 b) Y. Ishino, H. Shinagawa, K. Makino, M. Amemura, A. Nakata, J. Bacteriol. 1987, 169, 5429–5433.
- [2] a) G. J. Knott, J. A. Doudna, Science 2018, 361, 866–869; b) A. Pickar-Oliver, C. A. Gersbach, Nat. Rev. Mol. Cell Biol. 2019, 20, 490–507; c) M. Adli, Nat. Commun. 2018, 9, 1911.
- [3] a) J. P. Broughton, X. Deng, G. Yu, C. L. Fasching, V. Servellita, J. Singh, X. Miao, J. A. Streithorst, A. Granados, A. Sotomayor-Gonzalez, K. Zorn, A. Gopez, E. Hsu, W. Gu, S. Miller, C. Y. Pan, H. Guevara, D. A. Wadford J S Chen, C. Y. Chiu, Nat. Biotechnol. 2020, 38, 870–874; b) M. Bao, Q. Chen, Z. Xu, E. C. Jensen, C. Liu, J. T. Waitkus, X. Yuan, Q. He, P. Qin, K. Du, ACS Sens. 2021, 6, 2497–2522; c) M. M. Kaminski, O. O. Abudayyeh, J. S. Gootenberg, F. Zhang, J. J. Collins, Nat. Biomed. Eng. 2021, 5, 643–656.
- [4] a) R. Aman, A. Mahas, M. Mahfouz, ACS Synth. Biol. 2020, 9, 1226–1233; b) Y. Li, S. Li, J. Wang, G. Liu, Trends Biotechnol. 2019, 37, 730–743; c) R. Bruch, G. A. Urban, C. Dincer, Trends Biotechnol. 2019, 37, 791–792; d) R. Bruch, J. Baaske, C. Chatelle, M. Meirich, S. Madlener, W. Weber, C. Dincer, G. A. Urban, Adv. Mater. 2019, 31, 1905311; e) T. Yu, S. Zhang, R. Matei, W. Marx, C. L. Beisel, Q. Wei, AIChE J. 2021, 67, e17365; f) R. Nouri, Y. Jiang, Z. Tang, X. L. Lian, W. Guan, Nano Lett. 2021, 21, 8393–8400.
- [5] O. O. Abudayyeh, J. S. Gootenberg, S. Konermann, J. Joung, I. M. Slaymaker, D. B. Cox, S. Shmakov, K. S. Makarova, E. Semenova, L. Minakhin, K. Severinov, A. Regev, E. S. Lander, E. V. Koonin, F. Zhang, *Science* 2016, 353, aaf5573.
- [6] J. Chen, F. Jiang, C.-W. Huang, L. Lin, Analyst 2020, 145, 5226–5231.

- [7] J. S. Gootenberg, O. O. Abudayyeh, J. W. Lee, P. Essletzbichler, A. J. Dy, J. Joung, V. Verdine, N. Donghia, N. M. Daringer, C. A. Freije, C. Myhrvold, R. P. Bhattacharyya, J. Livny, A. Regev, E. V. Koonin, D. T. Hung, P. C. Sabeti, J. J. Collins, F. Zhang, Science 2017, 356, 438–442.
- [8] J. S. Chen, E. Ma, L. B. Harrington, M. Da Costa, X. Tian, J. M. Palefsky, J. A. Doudna, *Science* 2018, 360, 436–439.
- [9] H. de Puig, R. A. Lee, D. Najjar, X. Tan, L. R. Soenksen, N. M. Angenent-Mari, N. M. Donghia, N. E. Weckman, A. Ory, C. F. Ng, P. Q. Nguyen, A. S. Mao, T. C. Ferrante, G. Lansberry, H. Sallum, J. Niemi, J. J. Collins, Sci. Adv. 2021, 7, eabh2944.
- [10] J. Joung, A. Ladha, M. Saito, N.-G. Kim, A. E. Woolley, M. Segel, R. P. Barretto, A. Ranu, R. K. Macrae, G. Faure, E. I. Ioannidi, R. N. Krajeski, R. Bruneau, M.-L. W. Huang, X. G. Yu, J. Z. Li, B. D. Walker, D. T. Huang, A. L. Greninger, K. R. Jerome, J. S. Gootenbery, O. O. Abudayyeh, F. Zhang, N. Engl. J. Med. 2020, 383, 1492–1494.
- [11] B. Ning, T. Yu, S. Zhang, Z. Huang, D. Tian, Z. Lin, A. Niu, N. Golden, K. Hensley, B. Threeton, C. J. Lyon, X.-M. Yin, C. J. Roy, N. S. Saba, J. Rappaport, Q. Wei, T. Y. Hu, Sci. Adv. 2021, 7, eabe3703.
- [12] M. J. Kellner, J. G. Koob, J. S. Gootenberg, O. O. Abudayyeh, F. Zhang, *Nat. Protoc.* 2019, 14, 2986–3012.
- [13] E. Pujadas, F. Chaudhry, R. McBride, F. Richter, S. Zhao, A. Wajnberg, G. Nadkarni, B. S. Glicksberg, J. Houldsworth, C. Cordon-Cardo, *Lancet Respir Med.* 2020, 8, e70.
- [14] Y. Dai, R. A. Somoza, L. Wang, J. F. Welter, Y. Li, A. I. Caplan, C. C. Liu, Angew. Chem. Int. Ed. 2019, 58, 17399–17405; Angew. Chem. 2019, 131, 17560–17566.
- [15] P. Fozouni, S. Son, M. D. de León Derby, G. J. Knott, C. N. Gray, M. V. D'Ambrosio, C. Zhao, N. A. Switz, G. R. Kumar, S. I. Stephens, D. Boehm, C.-L. Tsou, J. Shu, A. Bhuiya, M. Armstrong, A. R. Harris, P. .-Y. Chen, J. M. Osterloh, E. D. Crawford, A. S. Puschnik, M. Phelps, A. Kistler, J. L. DeRisi, J. A. Doudna, D. A. Fletcher, M. Ott, Cell 2021, 184, 323–333.
- [16] R. Hajian, S. Balderston, T. Tran, T. DeBoer, J. Etienne, M. Sandhu, N. A. Wauford, J.-Y. Chung, J. Nokes, M. Athaiya J Paredes, R. Peytavi, B. Goldsmith, N. Murthy, I. M. Conboy, K. Aran, *Nat. Biomed. Eng.* 2019, 3, 427–437.
- [17] J.-M. Pawlotsky, F. Negro, A. Aghemo, M. Berenguer, O. Dalgard, G. Dusheiko, F. Marra, M. Puoti, H. Wedemeyer, J. Hepatol. 2018, 69, 461–511.
- [18] a) J. M. Barletta, D. C. Edelman, N. T. Constantine, Am. J. Clin. Pathol. 2004, 122, 20–27; b) R. Arnaout, R. A. Lee, G. R. Lee, C. Callahan, A. Cheng, C. F. Yen, K. P. Smith, R. Arora, J. E. Kirby, Clin. Infect. Dis. 2021, 73, e3042–e3046.
- [19] a) Y. Liang, M. Xiao, D. Wu, Y. Lin, L. Liu, J. He, G. Zhang, L.-M. Peng, Z. Zhang, ACS Nano 2020, 14, 8866–8874; b) Y. Yang, B. Zeng, Y. Li, H. Liang, Y. Yang, Q. Yuan, Sci. China Chem. 2020, 63, 997–1003.
- [20] W. Fu, L. Jiang, E. P. van Geest, L. M. C. Lima, G. F. Schneider, Adv. Mater. 2017, 29, 1603610.
- [21] a) M. T. Hwang, M. Heiranian, Y. Kim, S. You, J. Leem, A. Taqieddin, V. Faramarzi, Y. Jing, I. Park, A. M. van der Zande, S. Nam, N. R. Aluru, R. Bashir, *Nat. Commun.* 2020, 11, 1543; b) Y. Yang, X. Yang, X. Zou, S. Wu, D. Wan, A. Cao, L. Liao, Q. Yuan, X. Duan, *Adv. Funct. Mater.* 2017, 27, 1604096.
- [22] R. Bruch, G. A. Urban, C. Dincer, Nat. Biomed. Eng. 2019, 3, 419–420.
- [23] a) J. S. Gootenberg, O. O. Abudayyeh, M. J. Kellner, J. Joung, J. J. Collins, F. Zhang, *Science* 2018, 360, 439–444; b) P. Qin, M. Park, K. J. Alfson, M. Tamhankar, R. Carrion, J. L. Patterson, A. Griffiths, Q. He, A. Yildiz, R. Mathies, K. Du, ACS Sens. 2019, 4, 1048–1054.





- [24] A. Béraud, M. Sauvage, C. M. Bazán, M. Tie, A. Bencherif, D. Bouilly, *Analyst* 2021, 146, 403–428.
- [25] A. M. Fry, M. Chittaganpitch, H. C. Baggett, T. C. Peret, R. K. Dare, P. Sawatwong, S. Thamthitiwat, P. Areerat, W. Sanasuttipun, J. Fischer, S. A. Maloney, D. D. Erdman, S. J. Olsen, *PLoS One* 2010, 5, e15098.
- [26] Centers for Disease Control and Prevention 2020, https:// www.cdc.gov/coronavirus/2019-ncov/lab/rt-pcr-panel-primerprobes.html..
- [27] T. Y. Liu, G. J. Knott, D. C. Smock, J. J. Desmarais, S. Son, A. Bhuiya, S. Jakhanwal, N. Prywes, S. Agrawal, M. Díaz de León Derby, N. A. Switz, M. Armstrong, A. R. Harris, E. J. Charles, B. W. Thornton, P. Fozouni, J. Shu, S. I. Stephens, G. R. Kumar, C. Zhao, A. Mok, A. T. Lavarone, A. M. Escajeda, R. McIntosh, S. Kim, E. J. Dugan, I. T.
- Consortium, K. S. Pollard, M. X. Tan, M. Ott, D. A. Fletcher, L. F. Lareau, P. D. Hsu, D. F. Savage, J. A. Doudna, *Nat. Chem. Biol.* **2021**, *17*, 982–988.
- [28] L. Liu, Z. Xu, K. Awayda, S. J. Dollery, M. Bao, J. Fan, D. Cormier, M. R. O'Connell, G. J. Tobin, K. Du, *Adv. Mater. Technol.* 2022, 7, 2101550.
- [29] a) Z. Li, X. Ding, K. Yin, Z. Xu, K. Cooper, C. Liu, *Biosens. Bioelectron.* 2021, 192, 113498; b) H. Liu, A. Yang, J. Song, N. Wang, P. Lam, Y. Li, H. K.-w. Law, F. Yan, *Sci. Adv.* 2021, 7, eabg8387.

Manuscript received: March 14, 2022 Accepted manuscript online: May 12, 2022 Version of record online: May 31, 2022